

PACS numbers: 42.55.Ks; 42.60.Lh; 42.60.Jf
DOI: 10.1070/QE2005v035n04ABEH002875

Formation of the beam profile in a plate electrode HF laser

A.V. Andramanov, S.A. Kabaev, B.V. Lazhintsev, V.A. Nor-Arevyan,
A.V. Pisetskaya, V.D. Selemir

Abstract. **The near-field energy-density distribution of a beam from an HF electric-discharge laser with an inductively stabilised discharge, an SF_6- and H_2-based active medium, and interelectrode gaps of 34 and 52 mm is studied. Plates 1-mm thick and 60- or 120-mm wide oriented at an angle of 30° to the optical axis serve as 60-mm-wide electrodes. Electrodes 30-mm wide are formed by 60-mm-wide plates also oriented at an angle of 30° to the optical axis. The distributions of the laser-radiation density in a resonator with flat mirrors and the discharge-emission intensity over the resonator cross section are studied. The distributions of the laser-radiation density in the near-field zone and the discharge-emission intensity have similar profiles. The arrangement of the electrode plates at an angle of 30° provided a considerable increase in the width of the lasing region. The FWHM of the laser-radiation distribution is ~ 80 % of the electrode width for the both interelectrode gaps.**

Keywords: *HF electric-discharge laser, plate electrodes, inductive discharge stabilisation, discharge-emission intensity, laser-radiation distribution.*

1. Introduction

HF lasers based on plate electrodes with inductive discharge stabilisation have been developed in recent years [1 – 3]. The near-field radiation-density pattern for any laser is one of the basic characteristics that determine the fields of laser application. The distribution profile of the laser-beam energy density mainly depends on the energy-deposition distribution over the active-volume cross section and the type of the optical resonator used. The required distribution of the energy-deposition density at one-piece electrodes is formed by selecting appropriate profiles of their working surfaces [4]. As is known [5], applying profiled electrodes allows a substantial reduction of the electric-field inhomogeneity and an increase in the HF-laser efficiency. For plate electrodes, as well as for one-piece ones, the shape of the working edges of plates specifies the energy-deposition distribution in the working volume and the corresponding laser-beam profile [2, 3]. Specific features of the electrode unit, which consists of a set of anode – cathode pairs of plates, opens new possibilities for purposeful formation of the laser-beam profile. To effect additional possibilities in beam profiling, it is proposed to install electrode plates at an angle to the optical axis and to use plates with different profiles of the working edge in a single electrode unit.

The near-field laser-radiation density distribution for a resonator with flat mirrors is related to the energy-deposition distribution in the active-volume cross section. However, it is impossible to directly measure the distribution of the specific energy-deposition in the active volume. The specific energy-deposition in the discharge region also determines the intensity for visible light emitted by the discharge. In this work, we attempted to compare the near-field laser-radiation distribution to the distribution of the discharge-emission intensity over the active-volume cross section.

Studying the energy-density distribution over the HF-laser-beam cross section is a quite difficult problem that can be solved in several ways. The simplest method is to use a Spiricon digital pyroelectric camera. There are also special thermally sensitive photographic films (papers) that require subsequent photometric processing [6]. Here, we solved this problem using a well-known method of scanning the lasing region with a diaphragm and measuring the fraction of the laser-radiation energy transmitted through it.

The aim of this work was to study new possibilities of forming the laser-beam profile using a unit of plate electrodes with inductive discharge stabilisation in an HF laser.

2. Experimental results

A stainless-steel discharge chamber used in the experiments was 24 cm in diameter and 50 cm in length [2]. The electrode unit was installed inside it using feedthrough insulators. The chamber was closed with end metal flanges, to which two flat resonator mirrors ($R_1 = 100$ % and $R_2 = 35$ %) with an optical diameter of 50 mm were fastened.

Each electrode consisted of a set of mutually insulated copper electrodes 1-mm thick arranged at a certain spatial period. Three types of the profile of the electrode-plate working edge were studied. The plates with the first-type profile were 60-mm wide and had a radius of the working edge of 200 mm (the rounded edges of each plate had a 8-

A.V. Andramanov, S.A. Kabaev, B.V. Lazhintsev, V.A. Nor-Arevyan, A.V. Pisetskaya, V.D. Selemir All-Russian Scientific Research Institute of Experimental Physics – Russian Federal Nuclear Center, prosp. Mira 37, 607188 Sarov, Nizhni Novgorod region, Russia;
e-mail: mailbox@ntc.vniief.ru; web-site: http://www.vniief.ru

Received 23 September 2004; revision received 6 December 2004
Kvantovaya Elektronika **35** (4) 359 – 364 (2005)
Translated by A.S. Seferov

mm radius of curvature). The plates with the second-type profile were also 60-mm wide and had a working edge with Stappaers profile calculated for a 30-mm gap with coefficients $d_2 = 0.2$ and $d_4 = 0.8$ [4]. The plates with the third-type profile had a width of 120 mm and the same Stappaers profile.

Electrode units of several design versions were built on the basis of these electrode plates. In the first and second versions, 44 first-type (second-type) plates were installed normally to the optical axis with a special period of 6.5 mm along the electrode length. In the third version, 27 second-type plates were installed at an angle of 30° to the optical axis with a 9.1-mm period. In the fourth version, 21 third-type electrode plates were installed at an angle of 30° to the optical axis with a 9.1-mm period. Each cathode plate was installed in the plane of the corresponding anode plate; the distance between the working edges of the anode and cathode plates could be varied in the range 30 – 50 mm.

Figure 1 shows an electric circuit of the laser. The design of the electrode unit with 120-mm-wide plates oriented at an angle of 30° to the laser optical axis O_1O_2 is presented. Each of the cathode plates Π_i is connected to two common buses (CB_1, CB_2) of the pump source through two stabilising inductors $L_i \sim 500$ nH each. Plates 60-mm wide were connected to one of the two common buses through one stabilising inductor L_i.

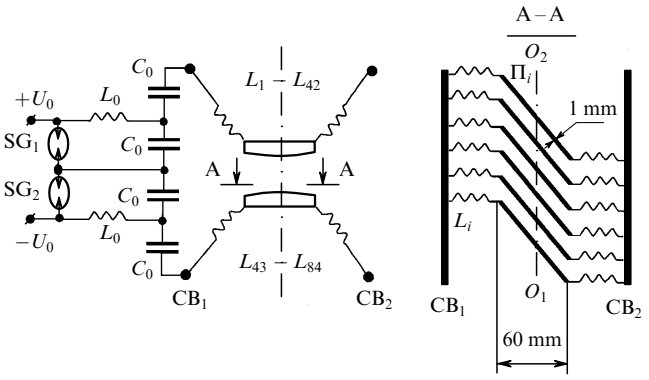

Figure 1. Electric circuit of an electric-discharge chemical laser.

The high-voltage generator of the pump source was assembled of 32 K15-24 capacitors (4.4 nF × 30 kV) according to a circuit of two *LC* generators and charged to a voltage of ± 20 kV from a bipolar power supply unit (Fig. 1 shows only a half of the pump source). After spark gaps $SG_1 - SG_4$ (RU-73) were enabled, a voltage with a rise time determined by the charge-exchange time of capacitors C_0 was applied to the discharge gap. Two ohmic dividers were simultaneously used to measure the voltage across the discharge gap. One divider was connected to three anode plates through three decoupling resistors (100 Ω), and the other was connected to three cathode plates in a similar manner. The discharge current was measured with a low-inductance shunt. Laser pulses were detected by an FSG-22 photodetector cooled with liquid nitrogen. A uniform diffuse sparkless discharge along the laser optical axis, which was initiated without preionising the working volume, was observed over a wide range of pressures in the working mixture.

Figure 2 shows typical oscillograms of voltage pulses across the discharge gap, as well as discharge-current and lasing pulses recorded by a TDS 3054 oscilloscope. A quasi-stationary discharge phase is clearly observed (Fig. 2a). A typical quasi-stationary electric-field strength in the inter-electrode gap $(E/P)_{st}$ observed in the experiments was ~ 90 kV cm^{-1} atm^{-1}. This value is typical of a chemical laser [7].

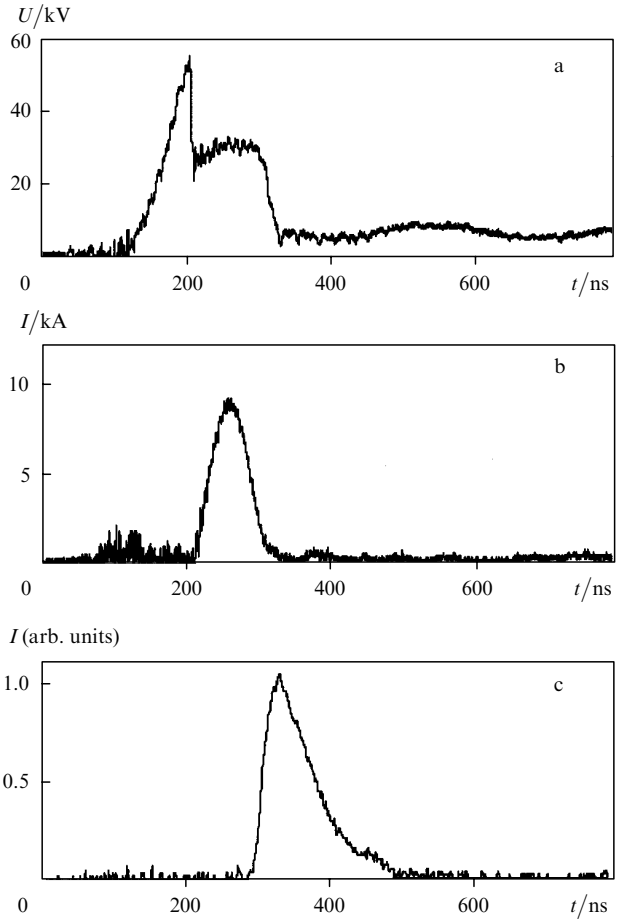

Figure 2. Oscillograms of (a) voltage pulses across the discharge gap, (b) discharge-current pulses, and (c) laser pulses for a 52-mm interelectrode gap at a total mixture pressure of 68 Torr. The mixture composition is $H_2 : SF_6 = 1 : 10$, the charging voltage is $U_0 = \pm 20$ kV.

The maximum discharge-current amplitude was 8.5 kA. The energy deposited in the discharge was 23 J, i.e., ~ 70 % of the energy stored in the capacitor bank. Lasing appeared ~ 100 ns after the beginning of the active-medium pumping. The laser-pulse FWHM was ~ 76 ns.

Figure 3 shows the optical layout of experiments for studying the HF-laser parameters. The distribution profile of the discharge-emitted visible light intensity in the active-volume cross section was recorded. To detect the discharge emission, the flange with the resonator mirror was replaced by a flange with an optical window with a 100-mm diameter, through which the discharge was photographed using an Olympus C4040Zoom digital camera. To increase the depth of focus, photographing was performed in parallel rays using lens (*4*) with a focal plane positioned at the centre of the discharge gap. The camera objective lens was focused to infinity. In the optical system in use, when the plane opti-

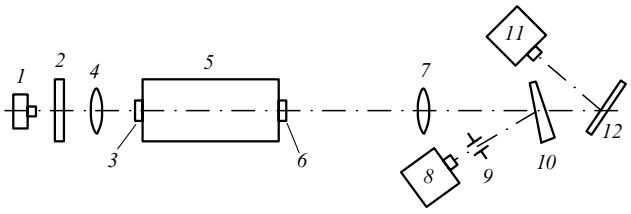

Figure 3. Scheme of the experimental setup: (*1*) digital camera; (*2*) light filter; (*3*) highly reflecting mirror; (*4*, *7*) lenses; (*5*) laser chamber; (*6*) output mirror; (*8*) pyroelectric calorimeter; (*9*) diaphragm; (*10*) optical wedge; (*11*) thermocouple calorimeter; and (*12*) reflecting plate.

cally conjugate to the plane of the camera array is displaced, the scale of its image on the array remained constant along the entire length of the discharge gap (to an accuracy of $\sim 3.5\,\%$). This optical arrangement allows correct recording of the discharge-emission intensity distribution over the active-volume cross section.

Typical photographs of the discharge emission in discharge gaps of height $d = 34$ and 52 mm at different configurations of installed electrode plates are shown in Fig. 4. One can see that the discharge is of volumetric character. The discharge width depends on the height of the discharge gap, the width of the electrode plates, and the angle of their setting. Streamers with dimensions and brightness that increase with an increase in the specific energy deposition are clearly observed near the cathode in all regimes. With a further increase in the specific energy deposition, streamers begin to develop from the anode as well (Fig. 4a). The maximum discharge width is ~ 50 mm (Fig. 4d).

Figure 5 shows typical photographs of the emission from the cathode electrode for plates installed perpendicularly

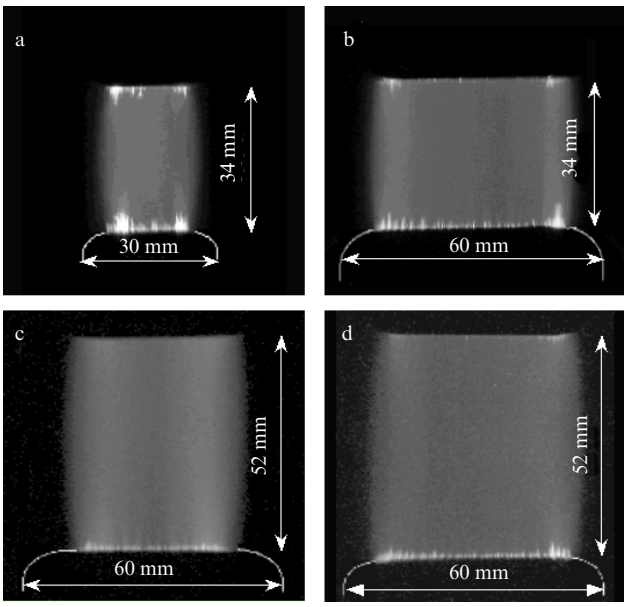

Figure 4. Photographs of the discharge emission in discharge gaps of 34 and 52 mm at a charging voltage $U_0 = \pm 20$ kV. Electrode plates with the Stappaers profile (a, c) 60- and (b, d) 120-mm wide are arranged at angles of (a, b, d) 30° and (c) 90° to the laser axis. The working mixture is $H_2 : SF_6 = 1 : 10$, the total pressure is (a, b) 84 and 68 Torr (c, d).

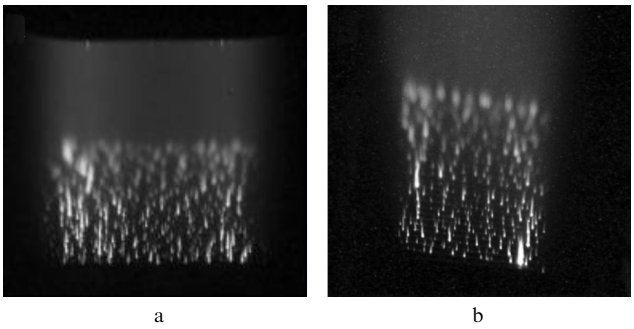

Figure 5. Photographs of emission from the cathode electrode in discharge gaps of (a) 34 and (b) 52 mm. Electrode plates with the Stappaers profile 60-mm wide are arranged at angles of (a) 90° and (b) 30° to the laser optical axis.

and at an angle of 30° to the laser optical axis. A typical structure of streamers is observed in these images. Streamers arise rather uniformly over the lengths of all plates and grow in size near the lateral sides of electrodes in regions with higher electric-field strengths.

The energy-density distribution over the laser-beam cross section was measured with ORIEL calorimeters (*8*) and (*11*) (Fig. 3). A nontransparent screen with a rectangular hole was applied to the laser output mirror for selecting an area of $\sim 15 \times 50$ mm in the central region of the discharge gap. An image of this region reduced by a factor of 4.7 was formed on a slit diaphragm of 10×0.3 mm using lens (*7*). Laser radiation passing through the diaphragm was incident on the receiving area of ORIEL 70271 pyroelectric calorimeter (*8*). ORIEL 70263 thermocouple calorimeter (*11*) detected either the radiation from the region that was not covered by the screen (to obtain the reference energy value) or the total laser energy, when the screen was removed. Figures 6 and 7 show the distributions of the laser energy density J over the width s of the interelectrode gap measured in these experiments.

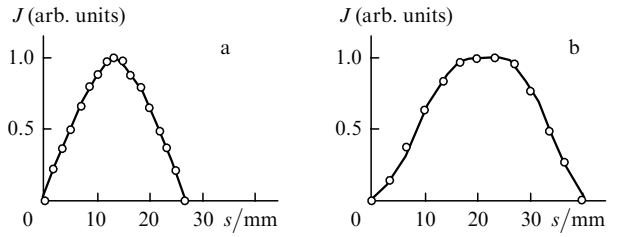

Figure 6. Distribution of the energy density J of laser radiation for discharge gaps of (a) 34 and (b) 52 mm at a 200-mm radius of the working edge of electrode plates.

Figure 7 also shows the results from the experiments for studying the discharge-emission intensity distribution over the active-volume cross section for electrode plates based on the Stappaers profile. The radiation intensities detected by individual pixels of the digital-camera array were averaged over the discharge-gap height in the region not shielded by the screen. To eliminate a background signal, photographing was performed in a darkened room. The linearity of the digital camera was tested using a set of neutral and colour glass filters for intensities $I - 0.1I$. The deviation from linearity was within 7 %.

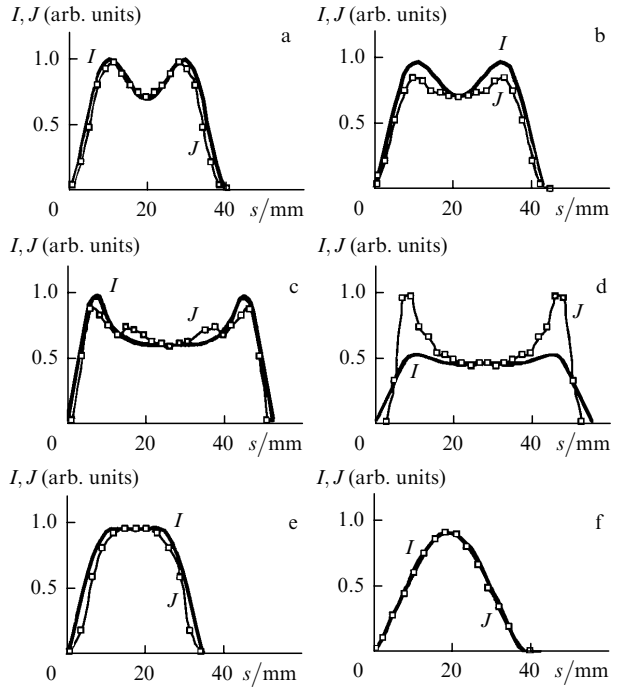

Figure 7. Distribution of the discharge-emission intensity I and the energy density J of laser radiation at a charging voltage $U_0 = \pm 20$ kV for discharge gaps of (a, c, e) 34 and (b, d, f) 52 mm, for which the electrode plates with the Stappaers profile (a, b, e, f) 60- and (c, d) 120-mm wide are arranged at angles of (a, b) 90° and (c–f) 30° to the laser optical axis.

The design of the electrodes did not allow equal spacings between electrodes to be set for the right and left parts of the interelectrode gap. The difference between these spacings on the lateral sides of the interelectrode gap was 0.20–0.35 mm in all cases. As a result, the laser-radiation density distribution and, correspondingly, the discharge-emission intensity distribution were asymmetric relative to the vertical plane of symmetry of the interelectrode gap. Figure 7 presents symmetrised distributions of these quantities (their average values at equal distances from the aforementioned plane on the right and left sides of the interelectrode gap). The forms of these distributions are determined only by the profiles of the working edges of electrode plates and are not related to the accuracy to which electrodes are installed. For comparison, Fig. 8 shows nonsymmetrised distributions.

An increase in the density of laser radiation on the lateral sides of the discharge gap (Fig. 7d) is associated with

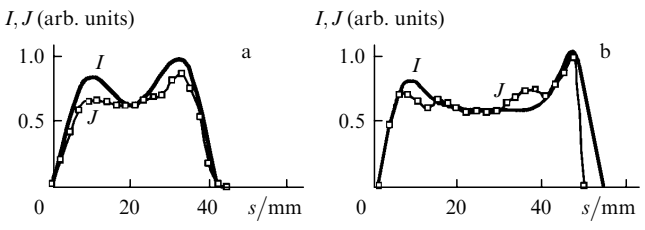

Figure 8. Nonsymmetrised distributions of the discharge-emission intensity I and the laser energy density J for discharge gaps of (a) 52 and (b) 34 mm. Electrode plates with the Stappaers profile (a) 60- and (b) 120-mm wide are arranged at angles of (a) 90° and (b) 30° to the laser optical axis.

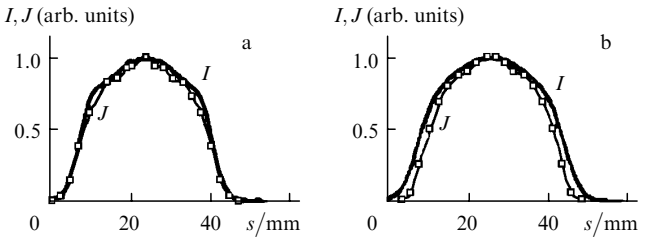

Figure 9. Distributions of the discharge-emission intensity I and the laser energy density J at a charging voltage $U_0 = \pm 20$ kV for discharge gaps of (a) 34 and (b) 52 mm obtained with electrode plates with the Stappaers profile 60-mm wide (22 pieces) and plates (22 pieces) with a 200-mm radius of the plates' working edge.

a mode of inversion accumulation in the discharge zone outside the laser resonator (the dimensions of the discharge zone is $\sim 52 \times 54$ mm, the optical diameter of the resonator mirrors is 50 mm). Radiation from the active volume situated outside the resonator was emitted due to a divergence of the laser beam at the mirror aperture, which led to an increased density of laser radiation near the mirror edge.

Using electrode plates with different profiles in a single electrode system allows one to attain additional possibilities for forming the required distribution of the energy deposition in the pump discharge and the corresponding output-energy density distribution over the laser-beam cross section. Figure 9 shows the distributions of the discharge-emission intensity and the output-energy density obtained with a combination of 22 first-type plates with a radius of the working edge $r = 200$ mm and 22 second-type plates with the Stappaers profile installed normally to the laser optical axis.

Figure 10 shows the distributions of the discharge-emission intensity in five cross sections distributed uniformly along the discharge-gap height. As can be seen in Fig. 10a, the distribution of the emission intensity changes insignificantly over the discharge-gap height, except for cross sections situated quite closely (at distances of ~ 5 mm) to the region occupied by streamers. Significant differences in the distribution profiles observed in Fig. 10b are associated with a considerable change in the pattern of electric fields along the interelectrode-gap height, when the spacing between the electrodes (52 mm) far exceeds their width (30 mm).

It follows from Figs 7–9 that the distribution profiles of the laser-energy density and the discharge-emission intensity

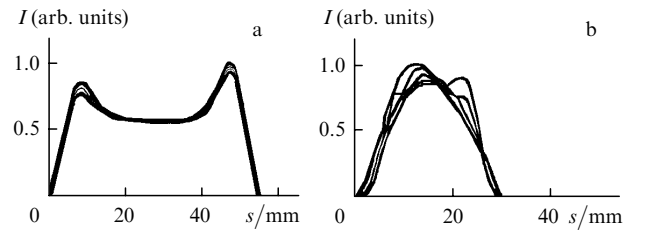

Figure 10. Distributions of the discharge-emission intensity I in five cross sections positioned uniformly along the height of discharge gaps of (a) 34 and (b) 52 mm. Electrode plates with the Stappaers profile (a) 120- and (b) 60-mm wide are arranged at an angle of 30° to the laser optical axis.

Table 1.

Plate width/mm	Angle to the optical axis/deg	Plate profile	$d = 34$ mm				$d = 52$ mm			
			E_{cr}/J	E_{lim}/J	E_c/J	E_{cr}/E_c	E_{cr}/J	E_{lim}/J	E_c/J	E_{cr}/E_c
60	90	Stappaers	0.71	0.27	0.83	0.86	0.77	0.09	0.69	1.12
60	90	Stappaers, $r = 200$ mm	0.88	0.25	0.81	1.09	0.81	0.15	0.88	0.92
120	30	Stappaers	0.71	0.15	0.78	0.91	0.53	0.06	0.58	0.91
60	30	Stappaers	0.75	0.21	0.79	0.95	0.81	0.13	0.86	0.94

coincide fairly well. Both the laser-energy density and the discharge-emission intensity are related to the specific energy deposition, and the good similarity of their distributions confirms the possibility of studying the distribution of the laser-energy density from the discharge-emission intensity distribution.

The laser output energy E_c that can be yielded by the entire active volume was calculated. These calculations were based on the laser output energy E_{lim} measured for a limited aperture (with an area of $\sim 15 \times 16$ mm) at the centre of the discharge gap and were performed for electrode plates with the Stappaers profile and a combination of 60-mm-wide plates with the Stappaers profile and $r = 200$ mm. The laser output energy E_c was found from the expression $E_c = E_{lim} \sum I / \sum I_{lim}$, where $\sum I_{lim}$ is the intensities summed up over the limited aperture and I is the intensities summed up over the entire discharge image. Table 1 presents the calculated values of energy E_c.

We then corrected the laser output energy E_m measured with the calorimeter from the 50-mm-diameter aperture of the resonator mirrors. When an appreciable part of the discharge image did not fall within the mirror aperture (see the distributions in Figs 7b–7d, 9b), the energy E_{cr} was found from the formula $E_{cr} = E_m \sum I / \sum I_s$, where $\sum I_s$ is the intensities summed up over the aperture of the resonator mirror. As a result, the energy E_m measured by the calorimeter increased by 1 % when using 120-mm-wide plates ($d = 34$ mm), by 6 % when using 60-mm-wide plates with the Stappaers profile ($d = 53$ mm), and by 3 % for a combination of plates with the Stappaers profile and $r = 200$ mm ($d = 52$ mm). Values of E_{cr} are also listed in Table 1.

This table shows that the ratio E_{cr}/E_c is close to unity for all versions of arrangement of electrodes. This indicates the possibility of estimating quite correctly the total laser energy on the basis of the values of the discharge-emission intensity and the laser output energy measured for a limited aperture. In the experiments described, the areas of the limited aperture were 16 %–25 % and 10 %–18 % of the discharge-image area for interelectrode gaps $d = 34$ mm and $d = 52$ mm, respectively.

Let us analyse the laser energy characteristics listed in Table 1. For a gap $d = 52$ mm, in which a quite homogeneous discharge with a weakly pronounced streamer structure is formed, a decrease in the discharge width is accompanied by an increase in the laser output energy. This indicates an insufficient laser-power density in the resonator for achieving an efficient inversion yield at a sufficiently high discharge cross sections. In this case, an efficient inversion yield is achieved by increasing the discharge-gap length [5]. As the laser-power density increases thanks to a change from $d = 52$ mm to $d = 34$ mm, the lasing energy also increases. This situation is realised for two types of electrodes: with 120-mm-wide plates and with a combination of plates with the Stappaers profile and plates with $r = 200$ mm, in which the discharge is homogeneous enough and the streamer structure is weakly pronounced. For electrode plates 60-mm wide with the Stappaers profile that are arranged perpendicularly and at an angle of 30° to the optical axis, the lasing energy is lower than for a gap $d = 52$ mm; this is caused by a less homogeneous discharge and a more pronounced streamer structure. However, even in this case, despite a quite developed streamer structure, the lasing energy increases with a decrease in the discharge width. The maximum lasing energy was achieved for electrodes with a combination of 60-mm-wide plates with the Stappaers profile and plates with $r = 200$ mm. This is evidently associated with the fact that, in this case, we managed to set virtually equal heights of discharge gaps over the entire electrode plane.

3. Conclusions

Our studies have shown that plate electrodes used jointly with an inductively stabilised discharge in HF lasers allow a new approach to a purposeful variation in both the distribution of the energy deposition over the active-volume cross section and the laser-beam profile in a resonator with flat mirrors. In addition to a conventional method based on a selection of an appropriate profile of the plates' working edges, several techniques were applied and their capabilities were tested.

One of these techniques includes the arrangement of electrode plates at an angle to the laser optical axis. For the same electrode width, the lasing region formed in this design is noticeably wider than for electrode plates arranged perpendicularly to the optical axis. In addition, plates with different profiles of the working edge can be used in a single electrode unit. It has been ascertained that, in this version, the laser-beam profile can be corrected; in particular, the radiation density can be levelled at the central part of the laser beam.

It is also shown that the intensity distribution of the discharge emission in the visible spectral region allows the profile of the output-energy density distribution over the active-volume cross section to be determined. This makes it possible to estimate the total output energy by measuring the laser energy emitted by a limited aperture, using the data on the recorded discharge-emission intensity. This approach is especially efficient for scaling wide-aperture electric-discharge lasers [3].

References

1. Lazhintsev B.V., Nor-Arevyan V.A. RF Patent No. 2105400, 12 November 1996; *Izobreteniya*, (5), 481 (1998).
2. Lazhintsev B.V., Nor-Arevyan V.A., Selemir V.D. *Kvantovaya Elektron.*, **30**, 7 (2000) [*Quantum Electron.*, **30**, 7 (2000)].
3. Andramanov A.V., Kabaev S.A., Lazhintsev B.V., Nor-Arevyan V.A., Selemir V.D. *Kvantovaya Elektron.*, **32**, 506 (2002) [*Quantum Electron.*, **32**, 506 (2002)].
4. Stappaers E.A. *Appl. Phys. Lett.*, **40**, 1018 (1982).
5. Panchenko A.N., Orlovskii V.M., Tarasenko V.F., Baksht E.Kh. *Kvantovaya Elektron.*, **33**, 401 (2003) [*Quantum Electron.*, **33**, 401 (2003)].
6. Aksenov Yu.N., Borisov V.P., Burtsev V.V., Velikanov S.D., Voronov S.L., Voronin V.V., Zapol'skii A.F., Kirülov G.A., Kovalenko O.I., Lazarenko V.I., Mis'ko V.M., Murugov V.M., Selemir V.D., Sin'kov S.N., Frolov Yu.N., Tsyberev V.P. *Kvantovaya Elektron.*, **31**, 290 (2001) [*Quantum Electron.*, **31**, 290 (2001)].
7. Apollonov V.V., Belevtsev A.A., Kazantsev S.Yu., Saifullin A.V., Firsov K.N. *Kvantovaya Elektron.*, **30**, 207 (2000) [*Quantum Electron.*, **30**, 207 (2000)].